Supplementary Information (SI) for Soft Matter.

Supporting Information for: Mikto-Grafted Molecular Brushes at Liquid Crystal-Aqueous Interfaces

Chiraz Toujani,[†] Ivana Herrera,[†] and Abelardo Ramírez-Hernández[*,†,‡]

†*Department of Biomedical Engineering and Chemical Engineering, The University of Texas at San Antonio, San Antonio, Texas 78249, USA.*

‡*Department of Physics and Astronomy, The University of Texas at San Antonio, San Antonio, Texas 78249, USA.*

E-mail: abelardo.ramirez-hernandez@utsa.edu

Liquid Crystals in the Bulk.

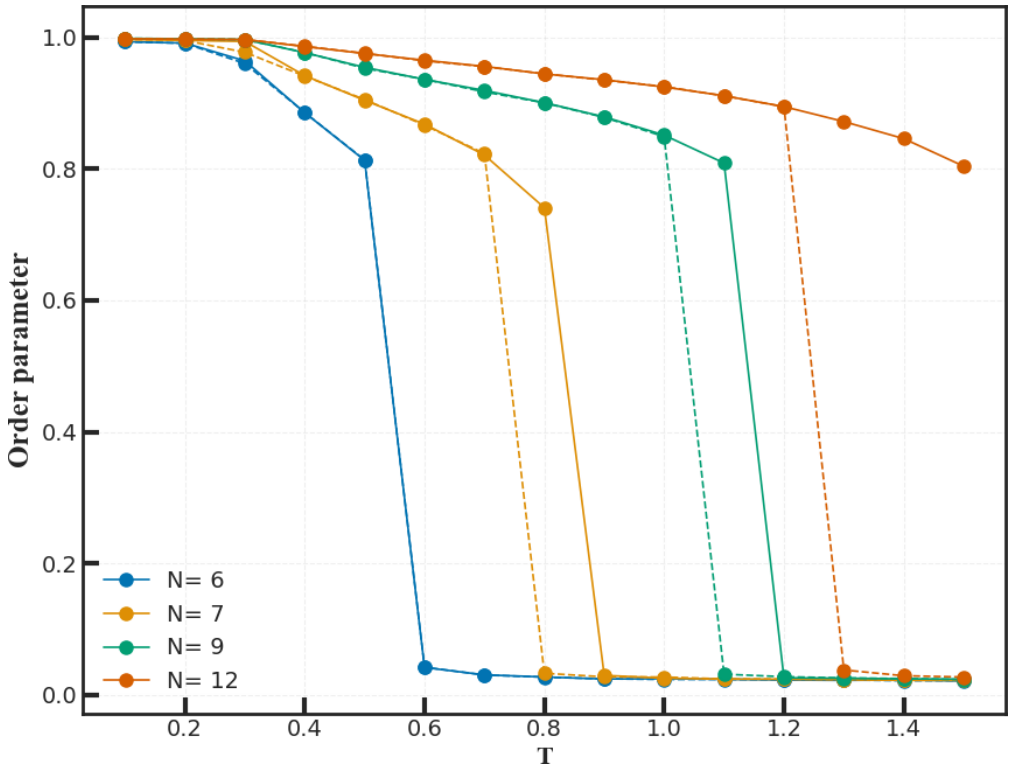

Figure S1: Average nematic order parameter of the liquid-crystal model, in the bulk, as a function of temperature; two thermal protocols were used: heating (solid lines) and cooling (dashed lines), for different mesogen lengths N.

Figure S1 displays the average nematic order parameter of the liquid crystals in the bulk as a function of temperature, evaluated under two thermal protocols. For $N = 9$ at $T = 1.0\ k_BT$, the liquid crystal displays a well-ordered nematic state.

Effect of the Backbone Length

Figure S2 presents the interfacial tension for backbone lengths $N_{bb} = 5$ (Fig. S2a) and $N_{bb} = 18$ (Fig. S2b). Consistent with the trends reported in the main text, increasing surfactant concentration leads to a reduction in interfacial tension, while longer sidechain lengths further enhance this decrease. Some deviations from the overall interfacial tension trends are observed and are attributed to metastable configurations that may require substantially longer simulation times to fully relax to equilibrium.

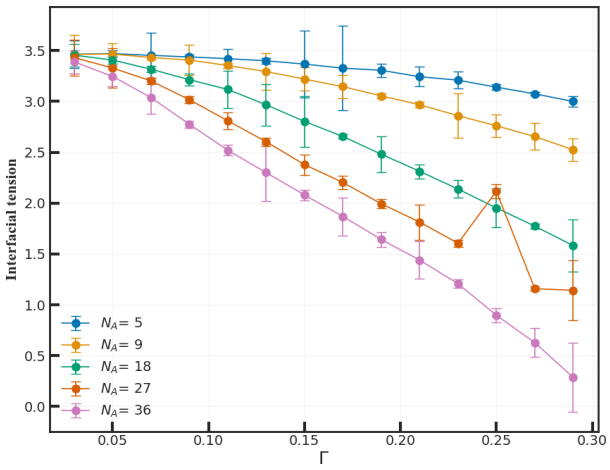

(a) $N_{bb} = 5$

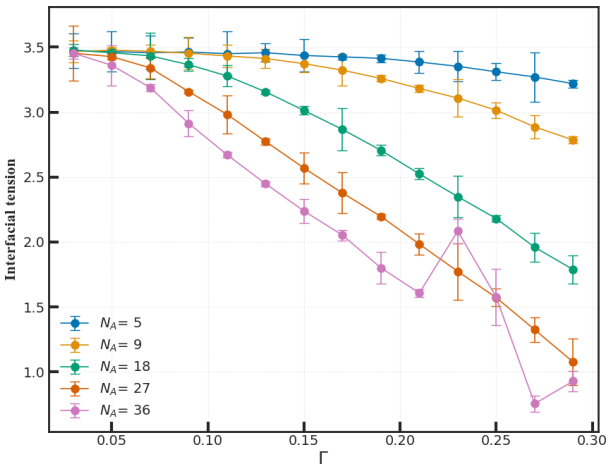

(b) $N_{bb} = 18$

Figure S2: Interfacial tension as a function of bottlebrush surface concentration, Γ, for different sidechain length for a fixed backbone length at (a) $N_{bb} = 5$ and (b) $N_{bb} = 18$.

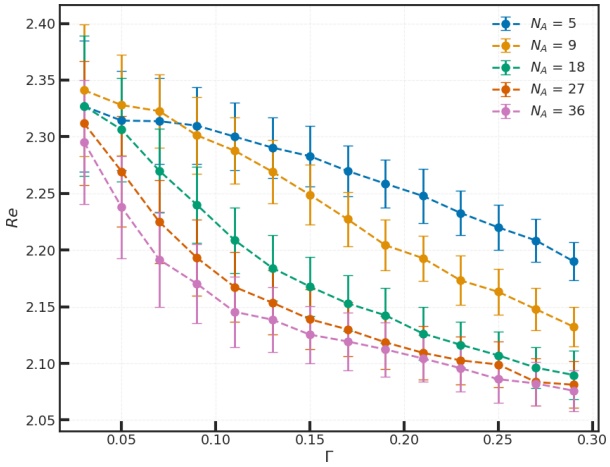

(a) $N_{bb} = 5$

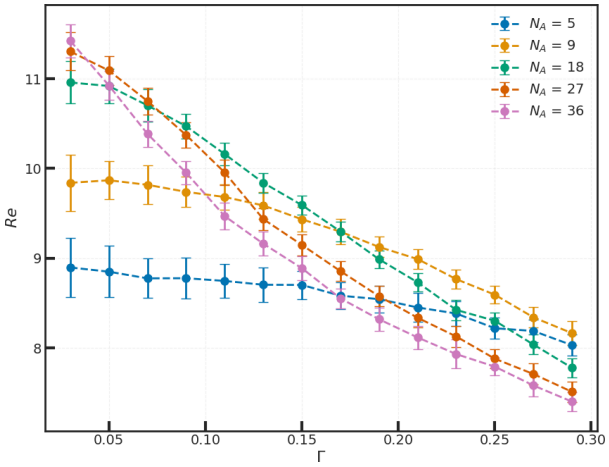

(b) $N_{bb} = 18$

Figure S3: End-to-end distance (Re) of the bottlebrush backbone as a function of concentration for different sidechain lengths, shown here for for a fixed backbone length at (a) $N_{bb} = 5$ and (b) $N_{bb} = 18$.

Figure S3 displays the backbone end-to-end distance as a function of surfactant concentration for varying sidechain lengths and backbone lengths, as indicated in the figure. A clear dependence on backbone length is observed. For the shortest backbone (Figure S3a), the influence of sidechain length is minimal, resulting in only a modest variation in the end-to-end distance (on the order of 0.5 n.u.). Moreover, the two distinct regimes identified in the main text corresponding to concentration ranges where sidechain length either influences or does not influence the backbone conformation are not clearly resolved at this backbone length. For $N_{bb} = 18$ (Figure S3b), the effect of backbone length becomes more pronounced. The two regimes associated with sidechain influence are clearly distinguishable, and the backbone end-to-end distance recovers the same qualitative trends discussed in the main text for $N_{bb} = 36$, with sidechain length exerting a systematic and concentration-dependent effect on backbone conformation.

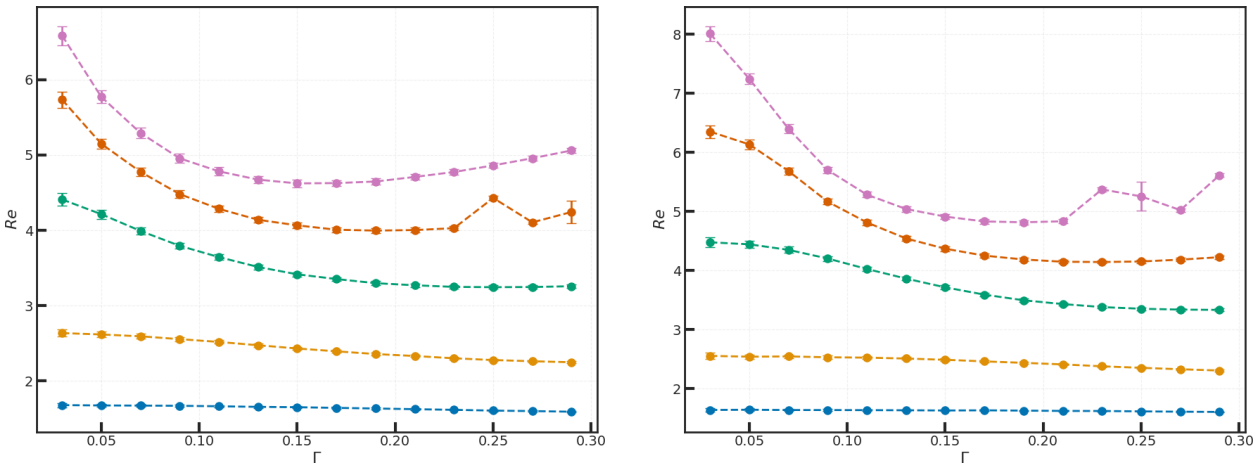

(a) $N_{bb} = 5$ (b) $N_{bb} = 18$

Figure S4: End-to-end distance (Re) of the bottlebrush **hydrophobic sidechains** as a function of concentration for different sidechain lengths, shown here for for a fixed backbone length at (a) $N_{bb} = 5$ and (b) $N_{bb} = 18$.

Figures S4 and S5 show the end-to-end distances of the hydrophobic and hydrophilic sidechains, respectively, as functions of surfactant concentration for different sidechain lengths and the indicated backbone lengths. The results follow the same qualitative trends reported in the main text for $N_{bb} = 36$.

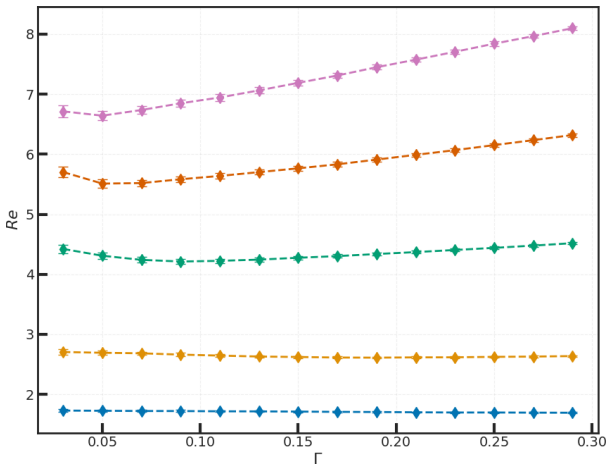

(a) $N_{bb} = 5$

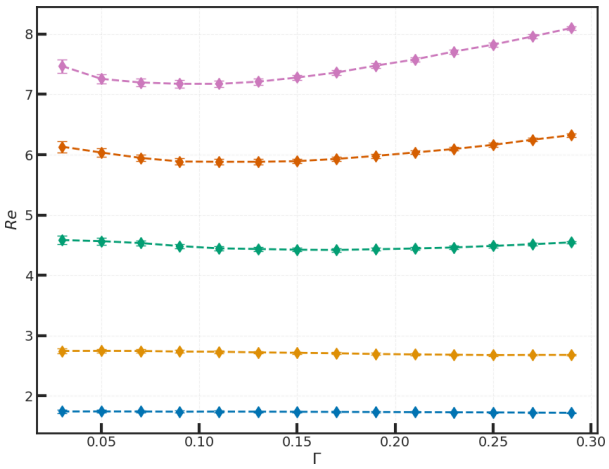

(b) $N_{bb} = 18$

Figure S5: End-to-end distance (Re) of the bottlebrush **hydrophilic sidechains** as a function of concentration for different sidechain lengths, shown here for for a fixed backbone length at (a) $N_{bb} = 5$ and (b) $N_{bb} = 18$.

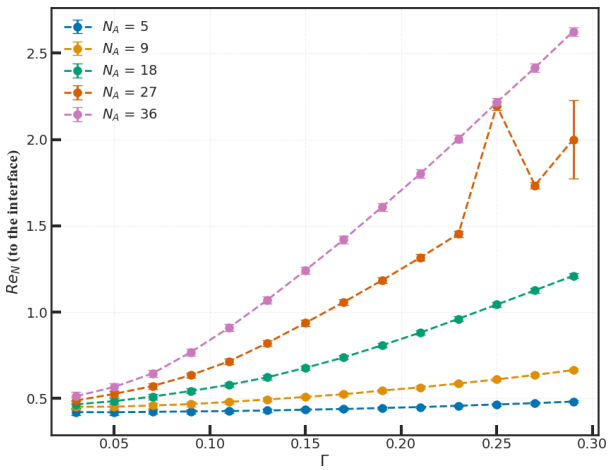

(a) Re_N

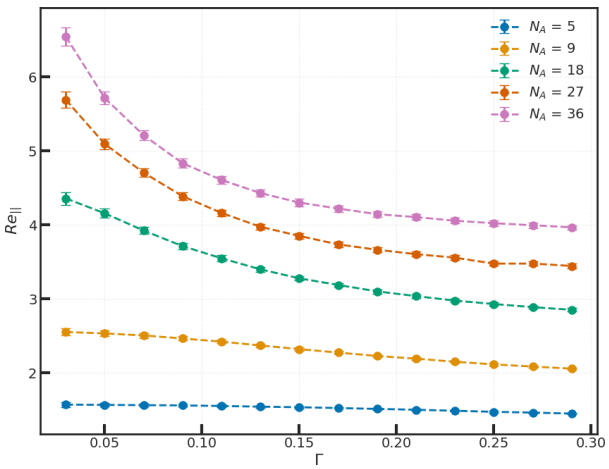

(b) $Re_{||}$

Figure S6: (a) Normal (Re_N) and (b) parallel ($Re_{||}$) component of the end-to-end vector of the bottlebrush **hydrophobic sidechains** as a function of concentration for different sidechain lengths, shown here for for a fixed backbone length at $N_{bb} = 5$.

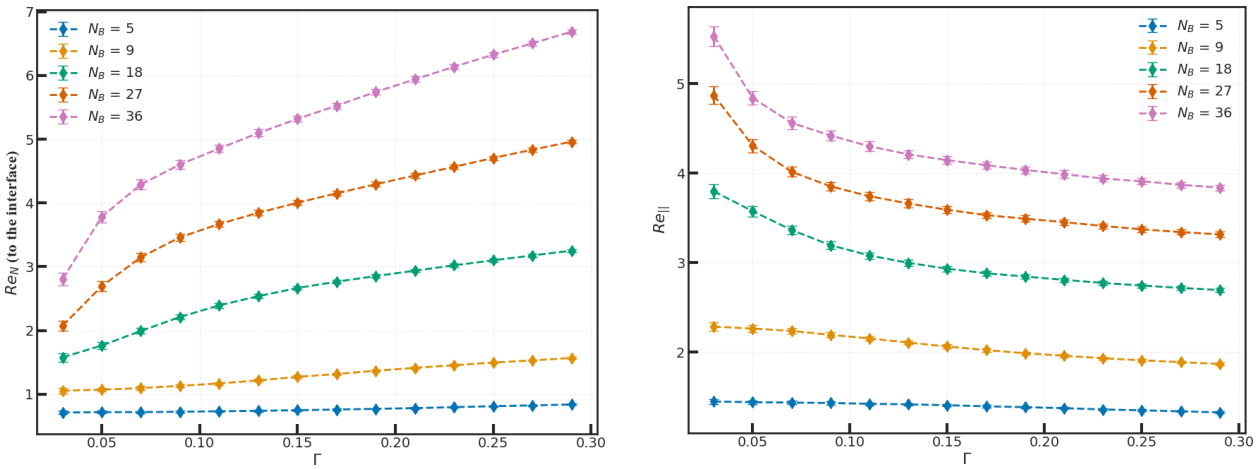

(a) Re_N (b) $Re_{||}$

Figure S7: (a) Normal (Re_N) and (b) parallel ($Re_{||}$) component of the end-to-end distance of the bottlebrush **hydrophilic sidechains** as a function of concentration for different sidechain lengths, shown here for for a fixed backbone length at $N_{bb} = 5$.

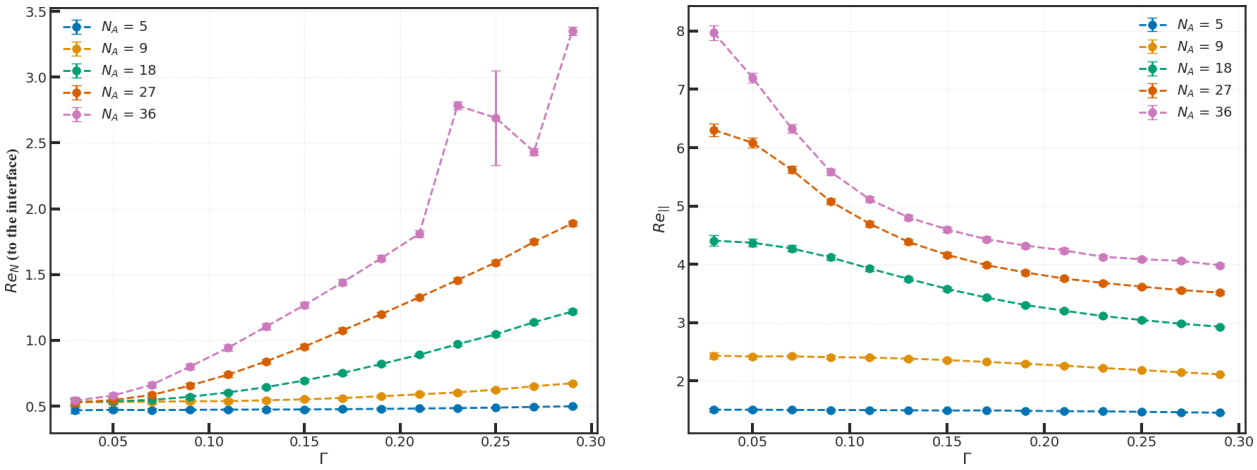

(a) Re_N (b) $Re_{||}$

Figure S8: (a) Normal (Re_N) and (b) parallel ($Re_{||}$) component of the end-to-end distance of the bottlebrush **hydrophobic sidechains** as a function of concentration for different sidechain lengths, shown here for for a fixed backbone length at $N_{bb} = 18$.

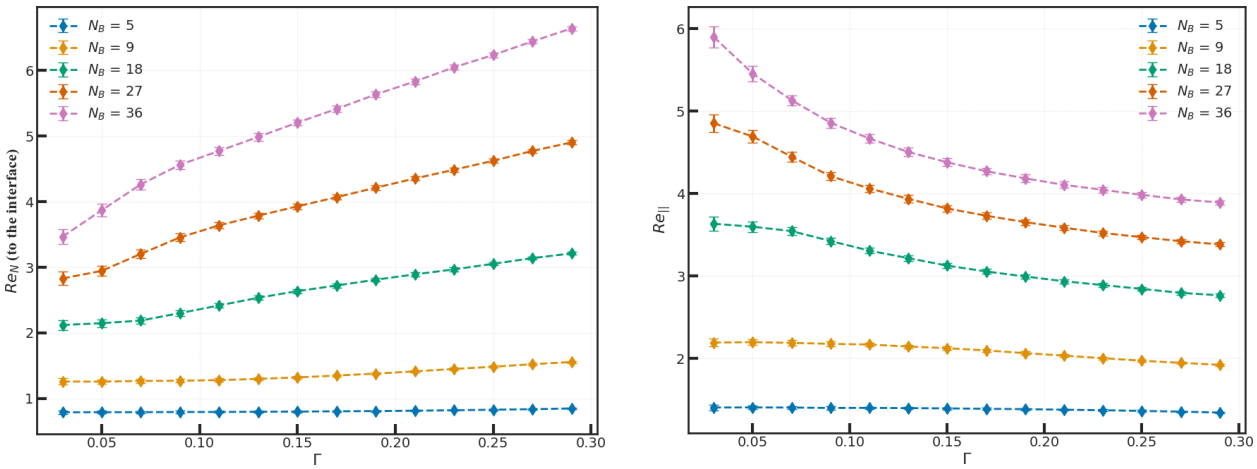

(a) Re_N (b) $Re_{||}$

Figure S9: (a) Normal (Re_N) and (b) parallel ($Re_{||}$) component of the end-to-end distance of the bottlebrush **hydrophilic sidechains** as a function of concentration for different sidechain lengths, shown here for for a fixed backbone length at $N_{bb} = 18$.

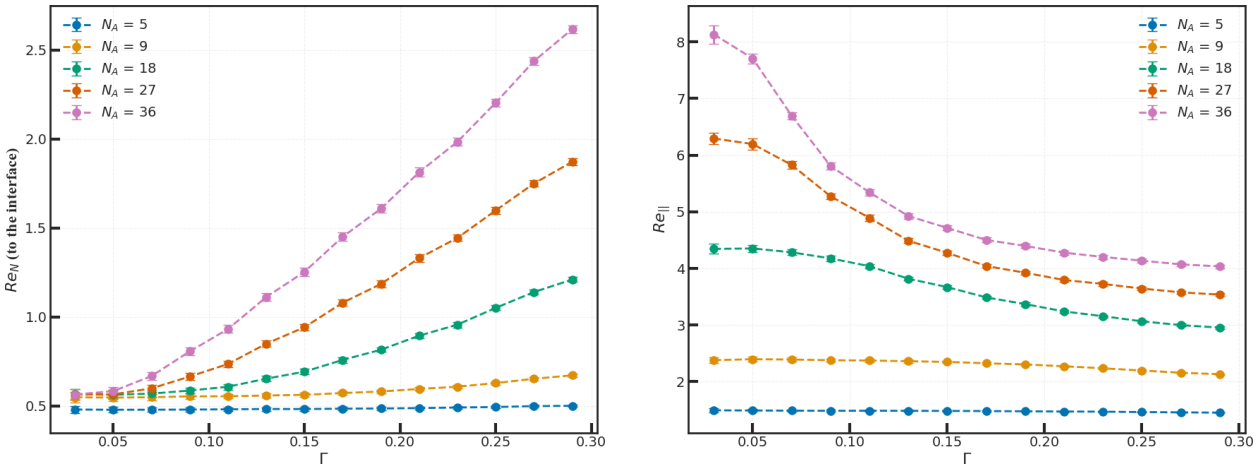

(a) Re_N (b) $Re_{||}$

Figure S10: (a) Normal (Re_N) and (b) parallel ($Re_{||}$) component of the end-to-end distance of the bottlebrush **hydrophobic sidechains** as a function of concentration for different sidechain lengths, shown here for for a fixed backbone length at $N_{bb} = 36$.

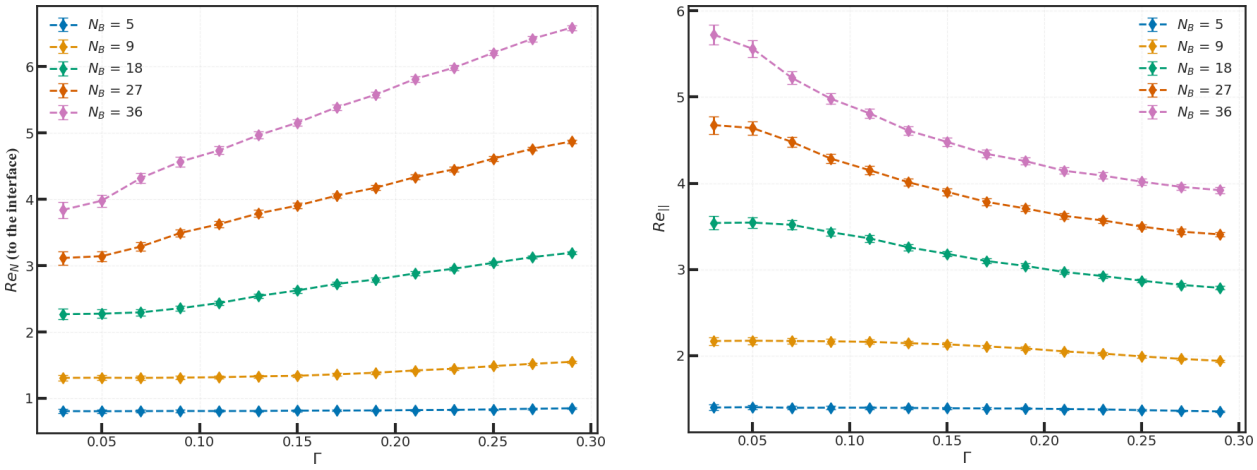

(a) Re_N (b) $Re_{||}$

Figure S11: (a) Normal (Re_N) and (b) parallel ($Re_{||}$) component of the end-to-end distance of the bottlebrush **hydrophilic sidechains** as a function of concentration for different sidechain lengths, shown here for for a fixed backbone length at $N_{bb} = 36$.

Figures S6–S11 display the parallel and normal components of the end-to-end vector for the hydrophobic and hydrophilic sidechains as functions of surfactant concentration, for different sidechain lengths at fixed backbone lengths (as indicated in the figure captions). Across all backbone architectures, a consistent trend is observed: the component parallel to the interface decreases with increasing concentration, while the component normal to the interface correspondingly increases. This behavior indicates a progressive reorientation of the sidechains away from the interface and toward the normal direction as both surfactant concentration and sidechain length increase, independent of backbone length.

Figure S12 shows the nematic order parameter as a function of bottlebrush concentration for the different sidechain and backbone lengths investigated. For both backbone lengths, only a modest decrease in the nematic order parameter is observed with increasing concentration and sidechain length. Deviations from this overall trend are limited to a small number of systems that remain trapped in metastable states, as discussed previously. Figure S13 presents top-view instantaneous snapshots of individual bottlebrushes at selected sidechain lengths and concentrations for a backbone length of $N_{bb} = 36$. At low concentrations, the hydrophobic sidechains are laterally extended along the interface. With increasing concen-

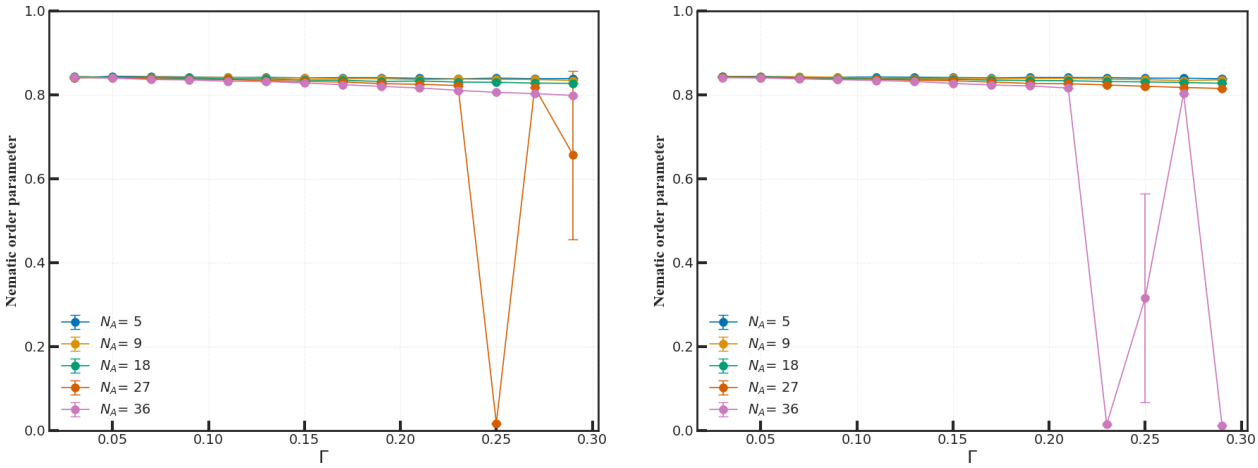

(a) $N_{bb} = 5$ (b) $N_{bb} = 18$

Figure S12: Nematic order parameter as a function of bottlebrush concentration Γ for different sidechain lengths while keeping backbone length fixed to (a) $N_{bb} = 5$ and (b) $N_{bb} = 18$.

tration, steric crowding from neighboring bottlebrushes becomes significant. Because the hydrophobic sidechains are unable to penetrate the liquid-crystal phase due to its rigidity, they undergo lateral compression at the interface, leading to a reduction in their end-to-end distance. Note that the stronger reduction in interfacial tension occurs when the polymer surface concentration is large enough that lateral interactions between neighboring chains become statistically significant. In this regime, polymers begin to form a more continuous interfacial layer, with partial overlap of their side chains and increased packing at the interface (see Figure S13). This collective organization enhances the screening of unfavorable LC–water contacts, which in turn leads to the observed decrease in the interfacial tension (see Figure 3 on the main text).

Figures S15 and S16 show the time evolution of the potential energy and interfacial tension for a representative system with a planar interface, demonstrating that both quantities reach a steady state and indicating that the system has attained equilibrium.

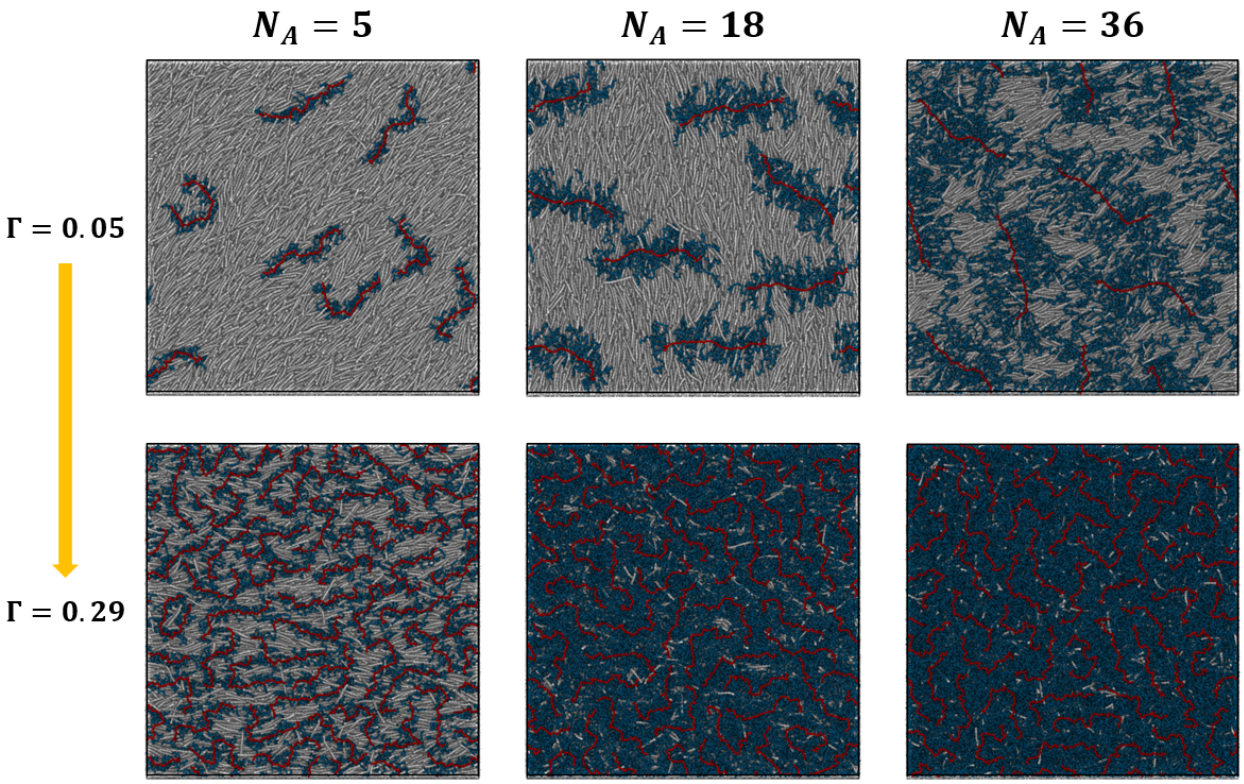

Figure S13: Top-view instantaneous snapshots of the bottlebrushes at selected sidechain lengths and concentrations. Hydrophilic sidechains and solvent have been removed for clarity.

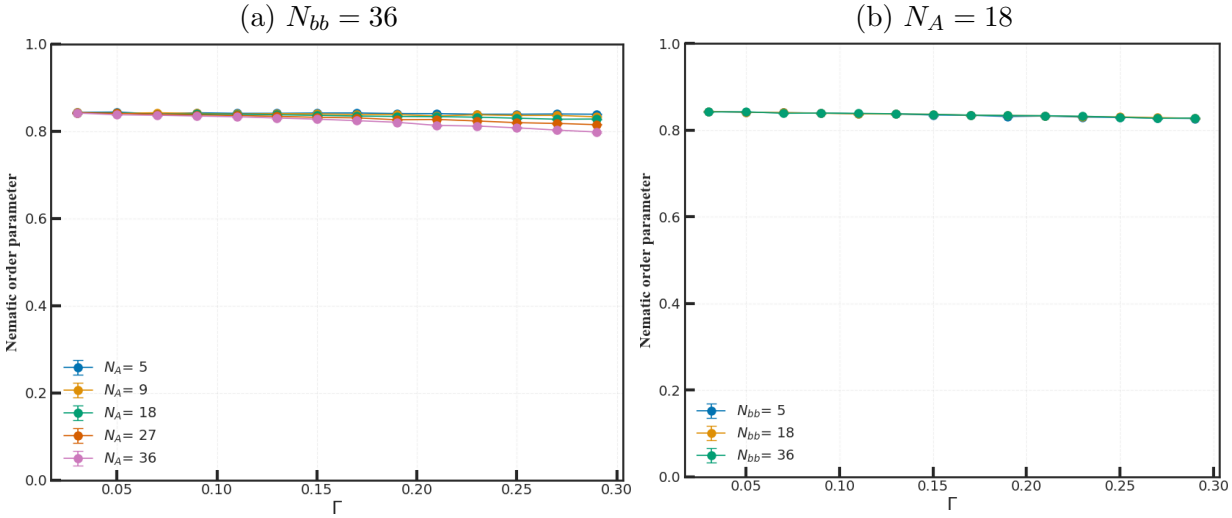

Figure S14: Nematic order parameter as a function of bottlebrush concentration Γ for (a) different sidechain lengths while keeping backbone length fixed to $N_{bb} = 36$ and (b) different backbone lengths while keeping sidechain length fixed ($N_A = 18$).

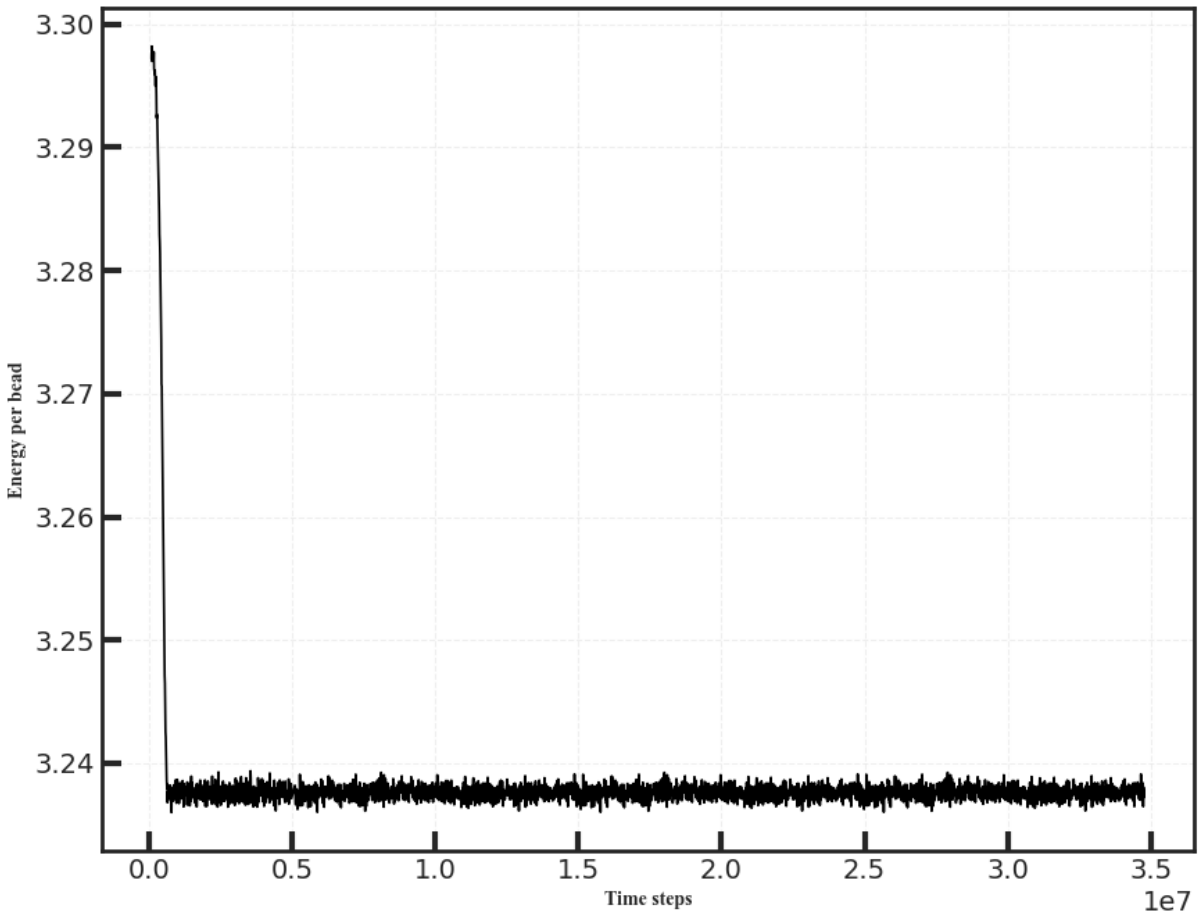

Figure S15: Time evolution of the potential energy for a selected system ($N_{bb} = 35$, $N_A = 27$ and $\Gamma = 0.29$).

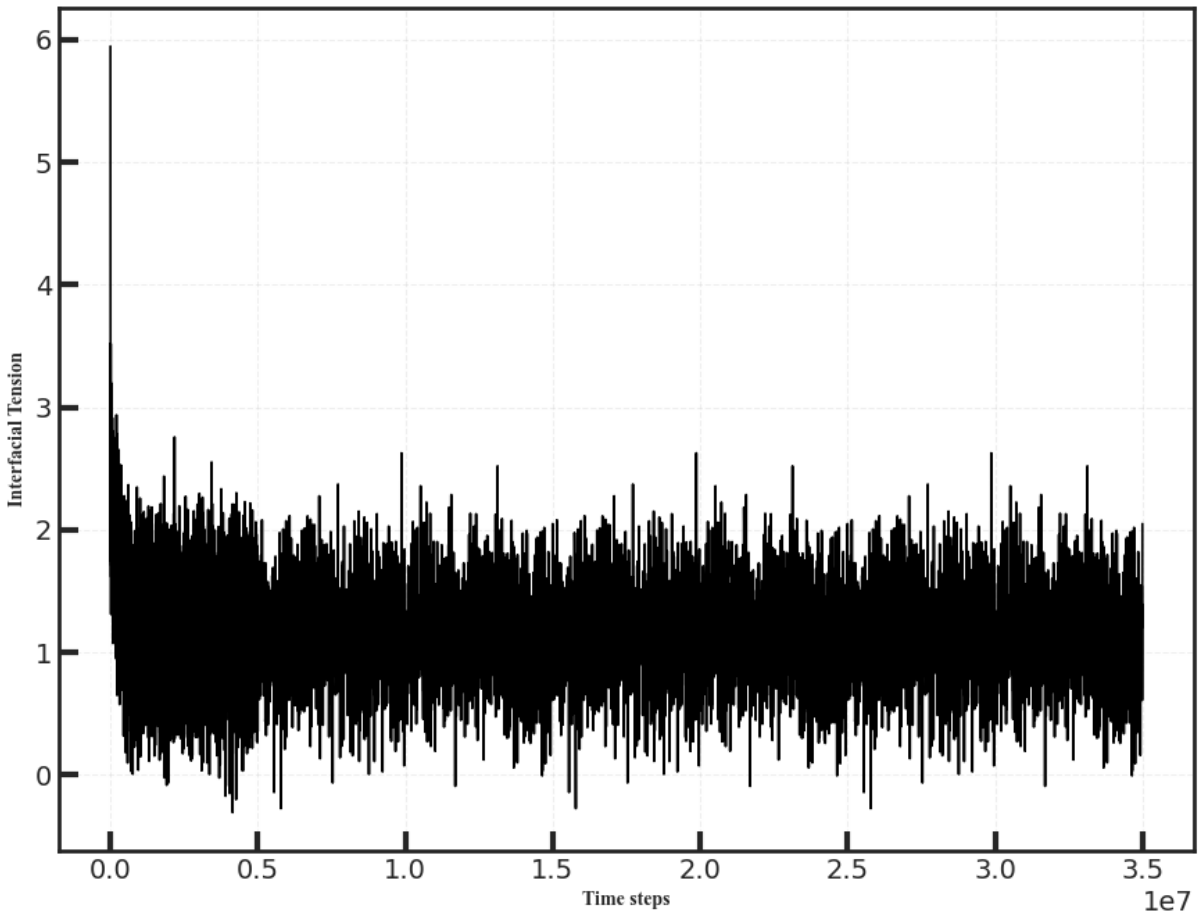

Figure S16: Time evolution of the interfacial tension for a selected system ($N_{bb} = 35$, $N_A = 27$ and $\Gamma = 0.29$).